7

Optical Conductivity and Spatial Inhomogeneity in Cuprate Superconductors

J. Orenstein

We present an overview of the microwave and millimeter wave response of cuprate superconductors, emphasizing two basic types of low-frequency optical conductivity, $\sigma(\omega)$, that these materials exhibit. The first type, exemplified by ultra-pure and stoichiometric $YBa_2Cu_3O_{7-\delta}$ (YBCO) single crystals, is well described by a single component originating from the Drude response of thermal quasiparticles. In other cuprate systems that have been studied $\sigma(\omega)$ has an additional component beyond the quasiparticle contribution, also centered at $\omega = 0$. The existence of this peak has not been widely appreciated because most of its spectral weight lies in the "terahertz gap" between microwave and infrared regimes. After reviewing the evidence for this spectral feature in a wide variety of cuprate compounds, we trace its origin to quenched spatial variation in the superfluid density, ρ_s. We show that the trends in optical conductivity as a function of hole carrier concentration in a series of $Bi_2Sr_2Ca_{1-y}Dy_yCu_2O_{8+\delta}$ (BSCCO) thin films can be understood by adding a component generated by spatial inhomogeneity to the quasiparticle Drude peak. We conclude by discussing the role of optical conductivity measurements in investigating the existence, origin, and importance of inhomogeneity in cuprate superconductors.

7.1. Introduction

7.1.1. Optical Conductivity of Superconductors

The dynamical conductivity, $\sigma(q, \omega)$, is the linear response function that relates current density to electric field. The $q \to 0$ limit of $\sigma(q, \omega)$ is referred to as the optical conductivity, or $\sigma(\omega)$, because it describes the response of the medium to electromagnetic waves with wavelength much longer than the characteristic length scales of condensed electronic systems. The real part of the optical conductivity, $\sigma_1(\omega)$, describes the dissipation of electromagnetic energy in the medium, while the imaginary part, $\sigma_2(\omega)$, describes screening of the applied field.

Measurement of $\sigma(\omega)$ in a superconductor is a powerful method for probing the dynamics of quasiparticle excitations and the size of the energy gap. According to BCS theory, there are three dissipative processes that determine $\sigma_1(\omega)$ in a superconductor: superfluid acceleration, pair creation, and quasiparticle scattering. The first is the work required to accelerate electrons to achieve the Meissner screening current. This contribution appears as a δ-function at zero frequency in $\sigma_1(\omega)$, whose spectral weight is the superfluid density, ρ_s. The latter

J. Orenstein • Physics Department, University of California, Berkeley, CA, USA
Materials Science Division, Lawrence Berkeley National Laboratory, Berkeley, CA 94720, USA

two contributions appear above zero frequency. In pair creation, electromagnetic energy is dissipated when a photon excites a pair of quasiparticles out of the BCS vacuum; in quasiparticle scattering the photon promotes a quasiparticle, already excited out of the vacuum due to thermal excitation, to a higher energy state.

7.1.2. Optical Conductivity and the Cuprates

Some special properties of the high-T_c cuprate superconductors make the study of $\sigma(\omega, T)$ particularly valuable in these materials. Because the gap is large, even relatively poor samples are in the clean limit where the scattering rate is smaller than the gap frequency, or $1/\tau \ll \Delta$. As a consequence the spectral weight associated with pair creation is very small and the contribution from quasiparticle scattering can be clearly resolved. Furthermore, $\sigma(\omega)$ associated with quasiparticle scattering can be quite accurately modeled by the Drude response of a dilute gas of weakly interacting particles [1]. This is not true of BCS s-wave superconductors, where the density of states singularity at the gap energy and the coherence factors strongly affect the conductivity spectra [2]. In d-wave superconductors, these influences are considerably weakened because there is a broad range of gap values extending from zero to the maximum gap, Δ_0.

The combination of clean-limit dynamics and d-wave density of states suggests that a simple two-fluid model (TFM) is applicable to $\sigma(\omega, T)$ in the cuprates. Because pair creation has vanishingly small spectral weight, the total conductivity should comprise only two components: the condensate δ-function and a Drude-like peak associated with thermal quasiparticles. The spectral weight of these two components are the normal and superfluid densities, or ρ_n and ρ_s, respectively. The conductivity sum rule requires $\rho_n(T) + \rho_s(T)$ to be independent of T.

The TFM does indeed provide an excellent overall description of the microwave properties of optimally-doped $YBa_2Cu_3O_{7-\delta}$ (YBCO) single crystals [3], particularly for temperature, T, above a few K. By fitting $\sigma(\omega, T)$ using the TFM, $\rho_s(T)$, $\rho_n(T)$, and $1/\tau(T)$, are determined [4]. However, the microwave properties of all other cuprate systems have turned out to be very different [5–9], showing clear indications of much greater disorder than YBCO. Even more significant is the fact that $\sigma(\omega)$ in these systems is inconsistent with the "dirty d-wave" picture [10], which provides a mean-field description of the effects of disorder on the conductivity.

According to the dirty d-wave picture, the quasiparticle spectrum is sensitive to disorder below a characteristic energy scale, E^* (or temperature scale, $T^* \equiv E^*/k_B$). For $E < E^*$ the density of states approaches a nonzero value, $N(0)$, at the chemical potential, while remaining linear in E above E^*. The existence of states at the chemical potential affects the low T properties of ρ_n and the quasiparticle conductivity. Instead of vanishing linearly with T, as expected for a clean d-wave superconductor, $\rho_n(T) \to \alpha T^* + \mathcal{O}(T^2)$ as $T \to 0$, where α is the temperature coefficient of $\rho_n(T)$ in the clean-limit. The residual quasiparticle spectral weight gives rise to conductivity that approaches a "universal" value $\sigma_d = (v_F/v_\Delta)\sigma_Q/\pi^2$ at low T (where $\sigma_Q \equiv e^2/\hbar d$ and d is the interplanar separation) [11, 12].

The dirty d-wave picture implies a correlation between the low T behaviors of ρ_s and ρ_n that is not observed in measurements on cuprates other than YBCO. In this article, we trace the inconsistency to the mean-field aspect of dirty d-wave, i.e., the assumption that disorder generates a nonzero $N(0)$ that is spatially homogeneous. Instead we argue that the density of states at the chemical potential, $N(0)$, and therefore both ρ_n and ρ_s, vary with position in the

medium [13]. This form of inhomogeneity changes qualitatively the nature of the optical properties, essentially by invalidating the selection rule that forbids coupling of the longitudinal excitations of the order parameter to $\sigma(\omega)$. The plausibility of an explanation for anomalies in $\sigma_1(\omega, T)$ based on spatial inhomogeneity has been strengthened by scanning tunneling microscopy (STM) measurements [14, 15]. The STM experiments demonstrate that the local density of states (LDOS) of $Bi_2Sr_2CaCu_2O_{8+\delta}$ (BSCCO) varies in space, with spatial fluctuations that have a minimum wavelength of $\sim$50 Å. The variations in LDOS suggest quenched inhomogeneity in local carrier concentration, x, and therefore in the local ρ_s.

The purpose of this article is to describe what can be learned from microwave and millimeter-wave (terahertz) spectra of cuprate superconductors whose $\sigma(\omega, T)$ cannot be described by a mean-field picture of disorder. The presentation is organized as follows. In Section 7.2 we compare the YBCO microwave data with results obtained on other optimally doped cuprates, highlighting qualitative differences in $\sigma(\omega, T)$. Section 7.3 presents a survey of (some previously unpublished) THz spectra, as measured in films of BSCCO with hole concentration varying from under to overdoped. These results help to clarify the nature of the difference in low-frequency conductivity between YBCO crystals and other cuprates. We show that a second Lorentzian peak, in addition to the quasiparticle Drude response, is needed to describe the observed $\sigma(\omega, T)$ in this latter class of materials. The weight of this peak *increases with decreasing* T in proportion to the superfluid density, distinguishing it from the quasiparticle contribution to $\sigma(\omega, T)$. In Section 7.4 we discuss the origin of the additional component, suggesting that the proportionality to ρ_s implies a connection to quantum phase fluctuations of the superconducting order parameter. We argue that the spectral weight displaced from the condensate by quantum phase fluctuations is strongly enhanced in the presence of quenched spatial inhomogeneity in ρ_s. Through a simple model, we show that the spectrum of the displaced spectral weight depends on the spatial correlation of ρ_n and ρ_s variations in the the medium. Specifically, the spectrum shifts from the plasma frequency to near zero frequency as the correlation varies from positive (such that regions of large ρ_s have large ρ_n) to negative (regions with large ρ_s have small ρ_n). In the last part of Section 7.4 we compare the theoretical modeling with the measured $\sigma(\omega, T)$. Finally, in Section 7.5 we discuss the relevance of the low-frequency optical conductivity to the debate over the origin and role of inhomogeneity in the cuprates, and indicate directions for future research.

7.2. Low Frequency Optical Conductivity in the Cuprates

7.2.1. YBCO Single Crystals: Success of the Two-Fluid Model

Detailed microwave studies of $\sigma(\omega, T)$ in high quality YBCO single crystals have been performed by the UBC group. Up to date reviews of this research have been provided by Bonn and Hardy (this volume) and by Maeda et al. [5]. Two sets of measurements exemplify the behavior of these materials. Figure 7.1 shows σ_1 of an optimally doped crystal as a function of T for several representative frequencies that range from 1 to 75 GHz [3]. Figure 7.2 shows data obtained using an experimental technique that enables continuous scan of frequency [17]. Here $\sigma_1(\omega)$ is displayed for temperatures in the range from 1 to 9 K, also for an optimally doped sample.

The main features of the microwave conductivity in YBCO are in excellent agreement with the predictions of the TFM of a d-wave superconductor in the clean limit. For our purposes, the essential feature of the data is the T-dependence of the normal fluid spectral

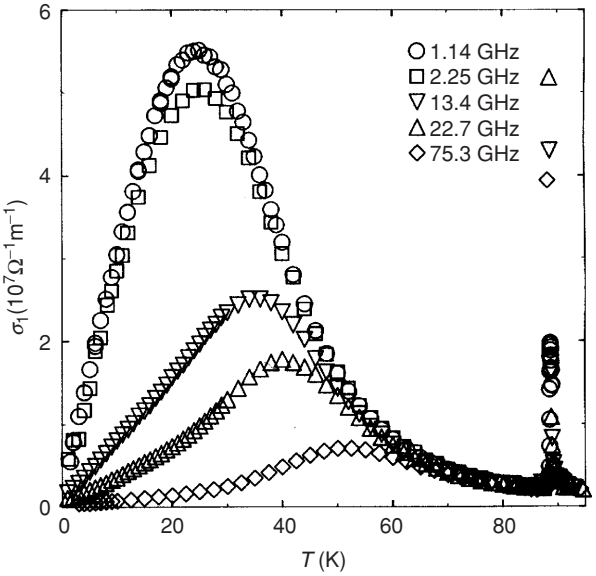

Figure 7.1. σ_1 vs. temperature for various frequencies in the microwave (GHz) range of the spectrum, as measured on a high-purity, optimally doped YBCO single crystal. From [3].

weight, which is depicted in the inset to Figure 7.2. As we will be discussing conductivity weight throughout this article, it is useful to settle on one consistent system of units throughout. The conductivity spectral weight is the integral of $\sigma_1(\omega)$ over ω. In the MKS system we can express spectral weight as the square of a plasma frequency through the relation, $\omega_p^2 = (2/\pi\epsilon_0)\int \sigma_1 d\omega$. Since for typical spectral weights we encounter, ω_p^2 expressed in s^{-2} is cumbersome, we suggest defining one spectral weight unit (SWU) as $10^{30}\,s^{-2}$. A superfluid condensate with 1 SWU corresponds to a London penetration depth of 300 nm. The London length in optimally doped YBCO (parallel to the a-axis) is approximately 150 nm, corresponding to 4 SWU.

According to the dirty d-wave model, the quasiparticle spectral weight that remains uncondensed is constrained by the relation $\rho_n(0) \simeq \alpha T^*$, where T^* is the T below which the increase of $\rho_s(T)$ is no longer linear. As indicated in the Figure 7.2 inset, $\rho_s(T)$ remains linear in this sample down to at least 1.3 K. Therefore, T^* can be no larger than 1 K and, taking $\alpha = 0.02$ SWU/K, dirty d-wave predicts that $\rho_n(0) < 0.02$ SWU. Referring to the solid symbols in the inset, we see that $\rho_n(0)$ calculated by direct numerical integration of the measured $\sigma_1(\omega)$ indeed satisfies this condition, extrapolating to less than 0.01 SWU as $T \to 0$. The maximum residual spectral weight is less than 0.25% of the condensate at $T = 0$.

As the residual spectral weight is so small, the conductivity at all temperatures above a few K satisfies the relation, $\rho_n(T) + \rho_s(T) = \rho_s(0)$. The above expression for the normal fluid spectral weight, together with a Drude conductivity spectrum,

$$\sigma_1(\omega, T) = \frac{\rho_n(T)\tau(T)}{1 + \omega^2\tau^2(T)}, \tag{7.1}$$

is sufficient to capture all the remarkable features of the quasiparticle conductivity seen in Figure 7.1 (1) the large peak in $\sigma_1(T)$ that occurs at temperatures below T_c, (2) the crossover

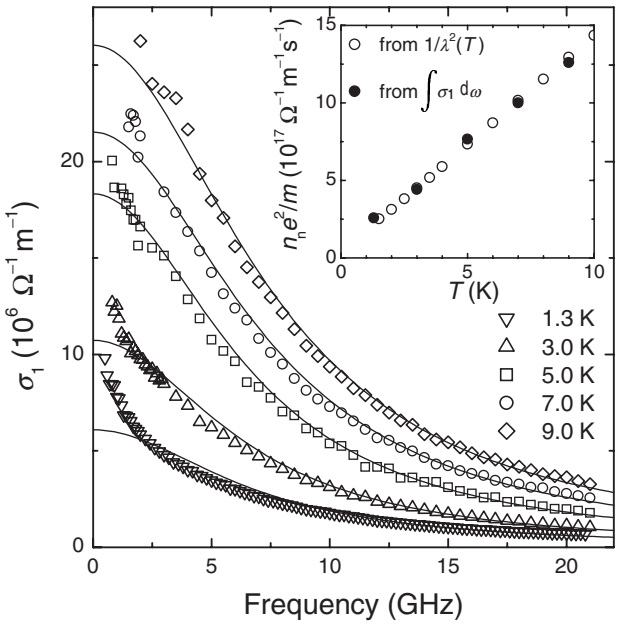

Figure 7.2. *Main panel:* σ_1 vs. frequency for several temperatures in the range 1.3–9.0 K, as measured on a high-purity, optimally doped YBCO single crystal. The solid lines show the best fit to the data obtained using the Drude model for the quasiparticle conductivity. *Inset:* The temperature dependence of the quasiparticle spectral weight as determined from numerical integration of the measured σ_1 and as inferred from the penetration depth. From [17].

of the peak T from ω-dependent to ω-independent behavior with decreasing frequency, and (3) the collapse of $\sigma_1(T)$ at all frequencies to a single curve at high T [4]. According to Eq. (7.1), σ_1 approaches a frequency-independent value, $\rho_n \tau$, in the high T regime where $\omega\tau(T) \ll 1$, thus explaining (3). The increase in σ_1 with decreasing T in this regime indicates that τ increases faster than ρ_n decreases. This is the evidence for the famous "collapse" of the quasiparticle scattering rate upon entering the superconducting state [18, 19], an observation that plays a crucial role in theories of high-T_c superconductivity. Regarding features (1) and (2), Eq. (7.1) predicts that $\sigma_1(T)$ will start to decrease when τ begins to exceed ω^{-1}. This accounts for a frequency-dependent peak T. However, as the measurement frequency is made lower, it will eventually become smaller than the low T limit of $1/\tau$ determined by elastic scattering. In this regime, $\sigma_1(T)$ peaks when the increase of τ can longer overcome the decrease of ρ_n with decreasing T. The frequency scale at which the peak becomes T-independent ($\sim$10 GHz in YBCO), provides an estimate of the elastic scattering rate. Note that an elastic scattering rate of $2\pi \times 10$ GHz, together with a Fermi velocity of $\sim 2.5 \times 10^7$ cm s^{-1}, corresponds to mean-free-path in the neighborhood of several microns.

7.2.2. The BSCCO System: Failure of the Two-Fluid Description

In the BSCCO family of superconductors, $\sigma(\omega, T)$ has been studied in nearly as much detail as in YBCO crystals [5]. Figure 7.3 shows an example of microwave data on an optimally doped BSCCO crystal [6] presented in the same format as Figure 7.1. The differences are quite striking, especially considering that the BSCCO and YBCO samples have almost the same T_c. In BSCCO, $\sigma_1(T)$ is independent of ω in the same range of frequency where

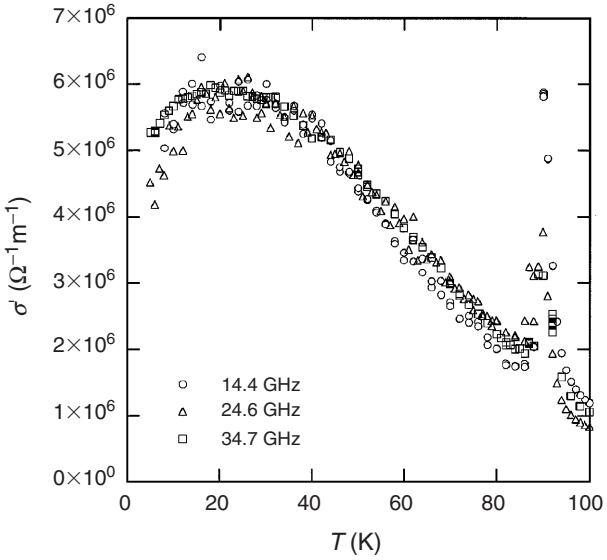

Figure 7.3. σ_1 vs. temperature for various frequencies in the GHz range, as measured in an optimally doped BSCCO sample. Note that the optical conductivity is independent of frequency throughout the same range that it depends strongly on frequency in YBCO. From [6].

$\sigma_1(T)$ in YBCO depends very strongly on ω. This contrast immediately suggests that $1/\tau$ is significantly larger in BSCCO as a result of increased disorder. However, despite the evidence for increased disorder, $\rho_s(T)$ increases linearly with decreasing T (see Figure 7.4) to at least 5 K [6, 7].

Based on these results, we can say that $\sigma(\omega, T)$ in BSCCO does not satisfy the conditions for internal consistency required by the dirty d-wave picture. From $\rho_s(T)$ we see that T^* cannot be greater than $\sim$3 K. Using the same value of α as in YBCO, dirty d-wave predicts an upper bound on $\rho_n(0)$ of 0.06 SWU. However, this is much smaller than the uncondensed quasiparticle spectral weight inferred directly from $\int \sigma_1(\omega)d\omega$. As σ_1 is ω-independent up to 35 GHz, the characteristic roll-off frequency of the Drude peak cannot be less than $\sim$100 GHz, placing a lower bound on $\rho_n(0)$ of $\sim$0.45 SWU. Thus, this BSCCO sample is highly ordered based on $\rho_s(T)$, but highly disordered based on $\rho_n(T)$.

THz spectroscopy performed on BSCCO films captures the frequency dependence of σ_1 that takes place above the range of microwave spectroscopy [20, 21]. In Figure 7.5 we show $\sigma_1(\omega, T)$ vs. T for an MBE-grown, slightly sub-optimally doped BSCCO thin film, for a series of representative frequencies from 150 GHz to 800 GHz. The lowest frequency THz data are quite similar to the highest frequency microwave data. Only above 150 GHz does σ_1 begin to change. These data prove that the essential frequency dependence of $\sigma_1(T)$ in BSCCO occurs at frequencies almost two orders of magnitude larger than in YBCO single crystals. Using these data, a more rigorous lower bound on $\rho_n(0)$ of 0.6 SWU is obtained by numerical integration of σ_1 up to 1 THz. *The uncondensed spectral weight in this sample is more than a factor of 60 larger than in the UBC-grown YBCO single crystals, and represents 30% of* $\rho_s(0)$.

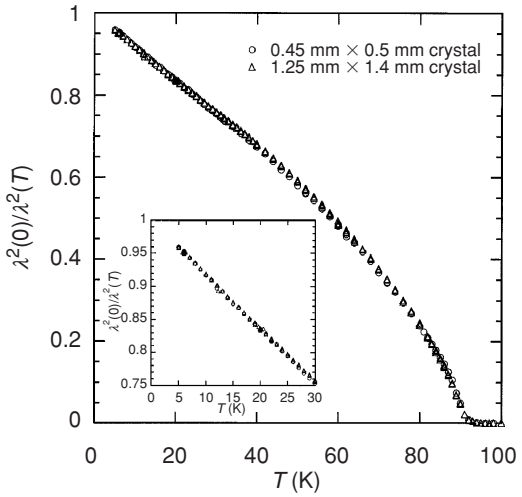

Figure 7.4. The temperature dependence of the inverse square of the penetration depth (proportional to the superfluid density, ρ_s), normalized to its value in the $T \to 0$ limit, for the same sample as Figure 7.3. $\rho_s(T)$ in BSCCO shows the same clean-limit behavior as YBCO, despite its much greater quasiparticle scattering rate. From [6].

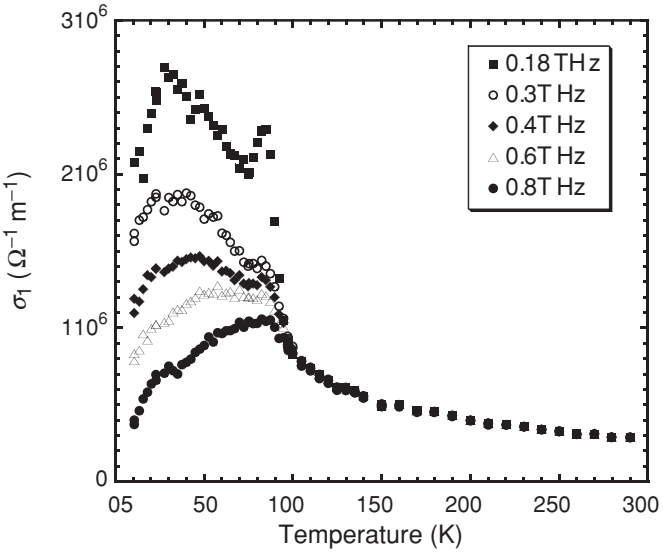

Figure 7.5. σ_1 vs. temperature for various frequencies in the THz range, as measured in a slightly underdoped BSCCO thin film with $T_c = 85$ K.

That $\rho_n(0)$ is comparable to $\rho_s(0)$ may be surprising to many readers. The more familiar picture of the optical conductivity in BSCCO comes from measurements of IR reflectivity, R, on bulk single crystals [22], an example of which is shown in Figure 7.6. Kramers–Kronig analysis of $R(\omega)$ provides an extremely accurate measurement of $\sigma(\omega)$ over a wide range

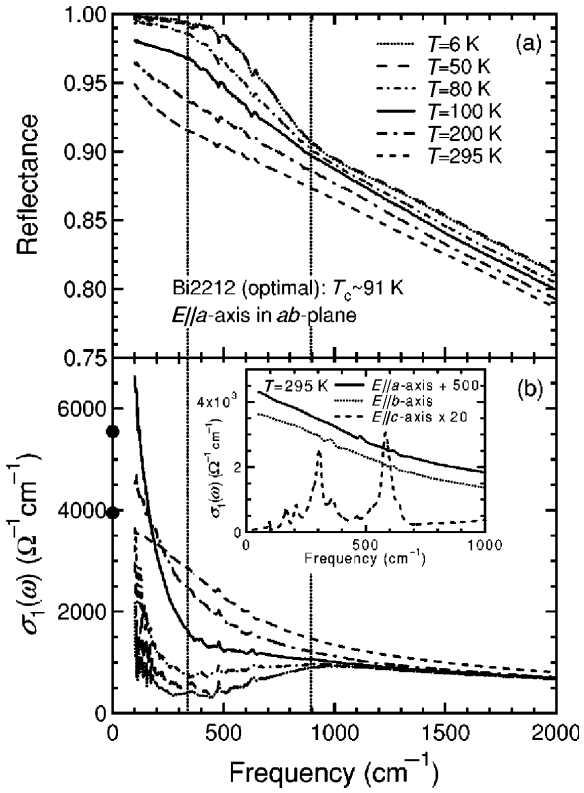

Figure 7.6. *Upper panel:* Reflectance as measured on an optimally doped BSCCO crystal as a function of frequency (in wavenumbers) at the temperatures indicated in the legend. *Lower panel:* Real part of optical conductivity as obtained by Kramers–Kronig transformation of the reflectance. From [22].

of frequency. However, the Kramers–Kronig analysis becomes unreliable when R becomes too close to unity, typically for frequencies below $\sim$100 cm^{-1}, or roughly 3 THz. As a result, IR reflection measurements are not sensitive to the low-frequency component of $\sigma(\omega)$ that is seen in microwave and THz spectroscopy. We note that this component, which approaches $6 \times 10^6\,\Omega^{-1}\,\mathrm{m}^{-1}$ as $\omega \to 0$, is a factor of 30 larger than the value of the conductivity at the low-frequency limit of IR reflectivity measurements.

A plot of σ_1 as a function of frequency from 0.01 to 100 THz, shown in Figure 7.7, presents a more complete picture of the low T optical conductivity of optimally doped BSCCO. The broad-band spectrum was assembled from microwave [6], terahertz [20], and infrared [22] data. For reference, the value of the universal d-wave conductivity is shown as a triangle symbol on the left-hand axis. Considering that the plot is a composite of data obtained from three different techniques (and three different samples), the continuity of $\sigma_1(\omega)$ is remarkable. The composite plot clearly demonstrates that the low T conductivity is dominated by a component centered at $\omega = 0$, with width $\sim$300 GHz.

For comparison, we show (in Figure 7.8) a composite of optical conductivity data as measured in optimally doped YBCO crystals (open symbols). The YBCO spectrum is

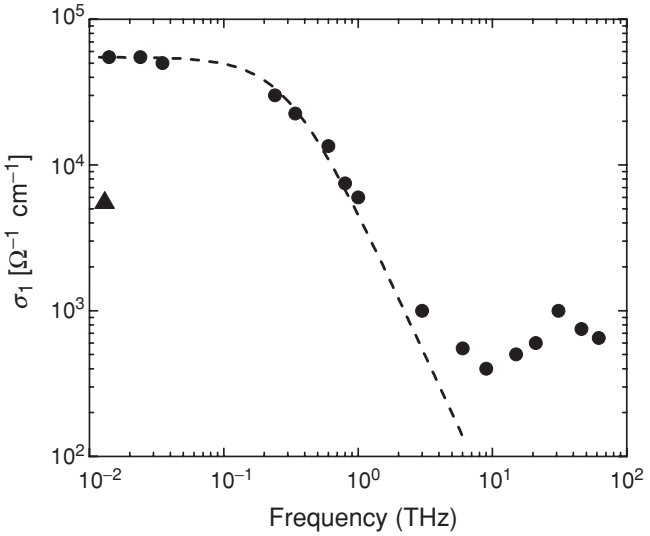

Figure 7.7. Composite plot of σ_1 at $T \leq 10\,\mathrm{K}$ as a function of frequency in THz. The spectrum is assembled from microwave [6], terahertz [20], and infrared [22] data. At low T the conductivity is dominated by a component centered at $\omega = 0$, with width $\simeq$300 GHz, whose magnitude as $\omega \to 0$ is much greater than the "universal d-wave conductivity" (triangle). The dashed line shows a Drude spectrum for scattering rate $(2\pi) \times 3 \times 10^{11}\,\mathrm{s}^{-1}$ and plasma frequency $1.1 \times 10^{15}\,\mathrm{s}^{-1}$, corresponding to 1.2 SWU in the units defined in the text.

assembled from microwave [3, 17] and infrared [23] data. The composite spectrum highlights several interesting features of the optical conductivity in YBCO. The conductivity in the low ω, T limit is comparable to that of optimal BSCCO and is larger than the universal d-wave value by a factor of approximately 20. In YBCO, the uncondensed spectral weight in the microwave region is much smaller than in BSCCO because the characteristic cutoff frequency is $\sim$3 GHz, compared with $\sim$300 GHz in BSCCO. However, we cannot conclude with certainty that the total uncondensed spectral weight in YBCO is small because, despite intense study of this material, ~~that~~ there is a large regime of frequency (0.08–3.0 THz) in which $\sigma(\omega)$ has not been measured. Moreover, a linear extrapolation of the power law decay of $\sigma(\omega)$ in the microwave regime to higher frequency far underestimates the conductivity at the low frequency limit of the infrared data. For purposes of illustration we have indicated (as a dashed line) one possible behavior of the conductivity in the THz regime. If the conductivity did indeed plateau near the universal d-wave value, the uncondensed spectral weight would be $\sim$0.2–0.3 SWU, which is still less than 10% of the condensate spectral weight in this material. Of course, the conductivity could, instead, exhibit a deep valley or large peak in the unmeasured frequency range.

7.2.3. Additional Examples

BSCCO is not the only example of a cuprate superconductor in which as much as one-third of the quasiparticle spectral weight remains uncondensed as $T \to 0$. Another example is optimally doped $La_{1-x}Sr_xCuO$ (LSCO), whose $\sigma(\omega)$ in the THz frequency regime has been

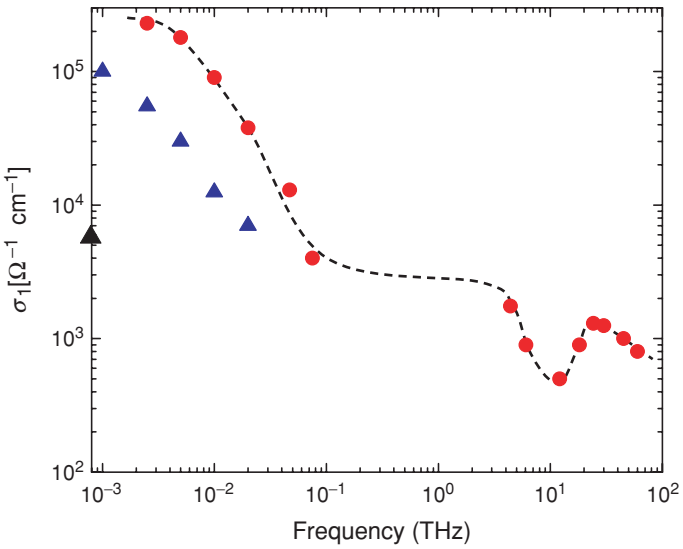

Figure 7.8. Composite plot of σ_1 in optimally doped YBCO, assembled from microwave [3, 17] and infrared [23] data. The blue and red symbols correspond to sample temperatures of 1.3 and 9 K, respectively. The line is a guide to the eye, illustrating one of the many possible ways that σ_1 could vary through the THz region where it has not been measured.

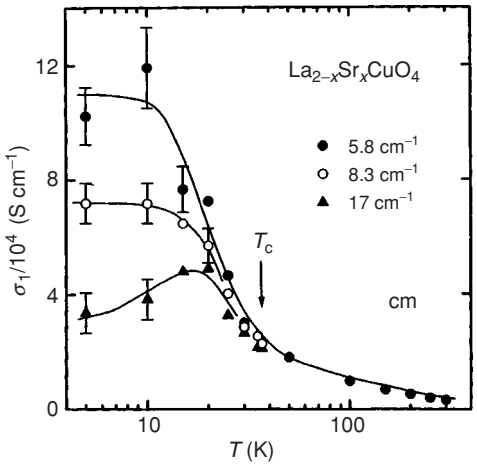

Figure 7.9. σ_1 vs. temperature for various frequencies in the THz range, as measured in an optimally doped thin film of LSCO with $T_c = 35$ K. The frequencies are given in wavenumbers, which can be expressed in Hz using the conversion 1 wavenumber = 30 GHz. From [8].

reported by Pronin et al. [8] (Figure 7.9). These authors analyze their data using a Drude model for the quasiparticle conductivity in which $\rho_n(T) + \rho_s(T)$ is constrained to be constant, but not necessarily equal to $\rho_s(0)$, thus allowing for the possibility of uncondensed quasiparticle spectral weight. From this analysis they conclude that $\rho_n(0)$ is *four times larger* than $\rho_s(0)$. The total spectral weight, $\sim$2 SWU, is nearly the same in LSCO as in BSCCO. However, the condensed portion in LSCO is only 0.4 SWU, which corresponds to a London length of 400 nm. Thus we see that the larger London length in LSCO, which is well known from other

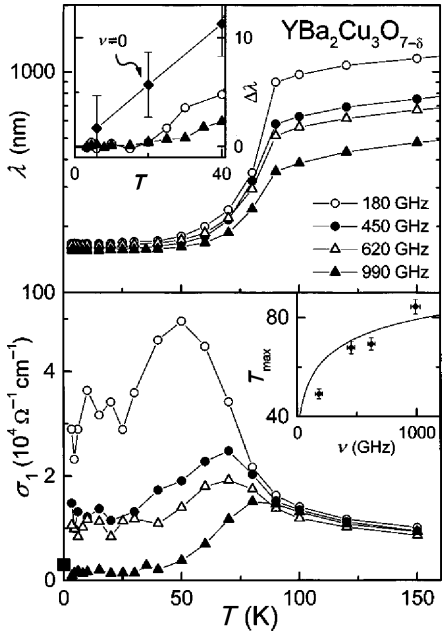

Figure 7.10. *Upper panel:* Dynamical penetration depth (proportional to $(\omega\sigma_2)^{-1/2}$ as a function of temperature for several frequencies in the THz regime. *Upper panel inset:* Penetration depth at low temperature plotted on a linear scale. Diamonds indicate extrapolation to zero frequency. *Lower panel:* σ_1 as a function of temperature for the same frequencies indicated in the upper panel. *Lower panel inset:* Positions of σ_1 peaks in frequency–temperature plane. From [25].

measurements [24], is not a consequence of smaller low-energy spectral weight, but rather results from the fact that only a small fraction of the low-energy spectral weight actually condenses to form the superfluid.

Another example of a system with a large residual spectral weight is YBCO in thin film form. The lower panel of Figure 7.10 shows $\sigma_1(T)$ in the THz regime for an optimally doped YBCO thin film [25]. These data show clearly the presence of uncondensed spectral weight in the $T \to 0$ limit. It is straightforward to estimate that $\rho_n(0) \simeq 1$ SWU, which is approximately one-third of the spectral weight that condenses. These results demonstrate that nearly compete condensation is not a general property of the YBCO system, but rather it is a unique property of ultra-pure, stoichiometric YBCO single crystals.

7.3. Optical Conductivity vs. Hole Concentration in BSCCO

7.3.1. Systematics of the Conductivity Anomaly

In this section we review THz conductivity measurements performed on a set of BSCCO films (which includes the optimally doped film discussed in Section 7.2) with varying hole concentration, x [20, 21, 26, 27]. The trends in $\sigma(\omega, T)$ with x clarify the nature of the uncondensed spectral weight. The data suggest strongly that an additional contribution to $\sigma_1(\omega)$, beyond the Drude response of quasiparticles, is required to understand the optical conductivity of the majority of cuprate samples.

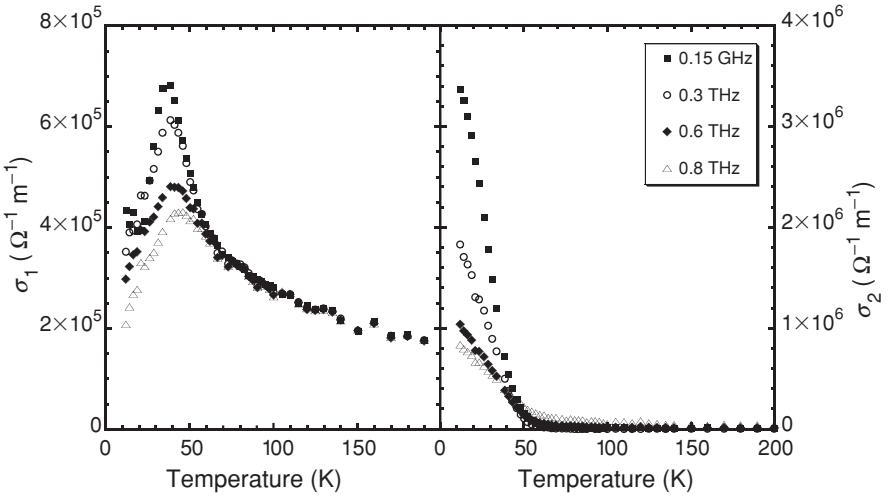

Figure 7.11. *Left panel:* σ_1 and *right panel:* σ_2 at the THz range frequencies indicated in the legend, as measured on an underdoped BSCCO thin film with $T_c = 51$ K. In contrast with optimally doped films, σ_1 peaks near T_c at all frequencies and the residual conductivity in the $T \to 0$ limit is small. The dynamical superfluid density, proportional to σ_2, is essentially linear with from low T to T_c.

The T_cs of the films range from 51 K (underdoped) to 75 K (overdoped). The real and imaginary parts of $\sigma(\omega, T)$ for each sample are presented, in the left and right-hand panels, respectively, in Figures 7.11, 7.12, and 7.13. To illustrate the trend most clearly, we first compare $\sigma(\omega, T)$ in the end members of the series, the most underdoped (Figure 7.11) and the most overdoped (Figure 7.13). In the overdoped sample $\sigma_1(\omega, T)$ is similar to that in the near-optimally doped sample discussed in Section 7.2. The peak in $\sigma_1(T)$ moves systematically to lower T with decreasing ω. However, σ_1 does not approach zero below the peak T; a substantial amount of spectral weight remains uncondensed in the limit that $T \to 0$. The THz conductivity of the most underdoped sample is markedly different, in that $\sigma_1(T)$ peaks just below T_c, independent of frequency. Moreover, spectral weight decreases at low T as expected for a clean d-wave superconductor. The σ_1 spectra for the intermediate sample ($T_c = 71$ K) follows the trend in that the low T dissipation, while clearly visible in the 100 GHz data, is much smaller than in the more heavily doped samples.

We next discuss why the Drude conductivity of superconducting quasiparticles is insufficient to model the $\sigma(\omega, T)$ observed in this set of BSCCO films. There are three basic reasons:

1. *The single component Drude spectrum cannot describe the ω and T dependence of σ.* A robust prediction of any single component model is that $\sigma_1(T)$ for all ω merge as $T \to T_c$ (as seen in the YBCO single crystal data). This prediction does not depend on a specific choice of frequency dependence for the quasiparticle peak, such as Lorentzian. It is seen in all single-component models because the initial increase in $\sigma(T)$ with decreasing T requires $\omega\tau \ll 1$ near T_c. In this limit $\sigma_1 \to \sigma(0, T)$, which is, of course, independent of ω. As is most clear in the spectra in the optimal and overdoped BSCCO films, $\sigma_1(T)$ at different ω fans out immediately below T_c, a feature which is at odds with the single component picture.

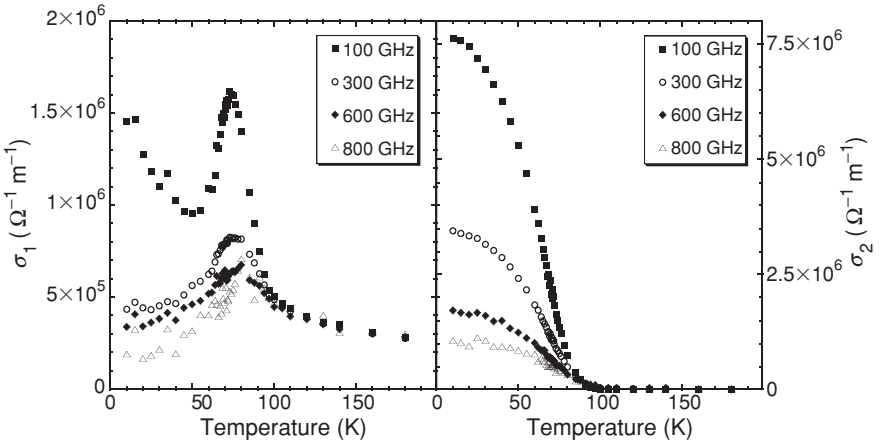

Figure 7.12. *Left panel:* σ_1 and *right panel:* σ_2 at the THz range frequencies indicated in the legend, as measured on an underdoped BSCCO thin film with $T_c = 71$ K. The behavior of σ_1 is intermediate between that of very underdoped and optimal samples in that the residual conductivity is apparent only at the lowest measurement frequency.

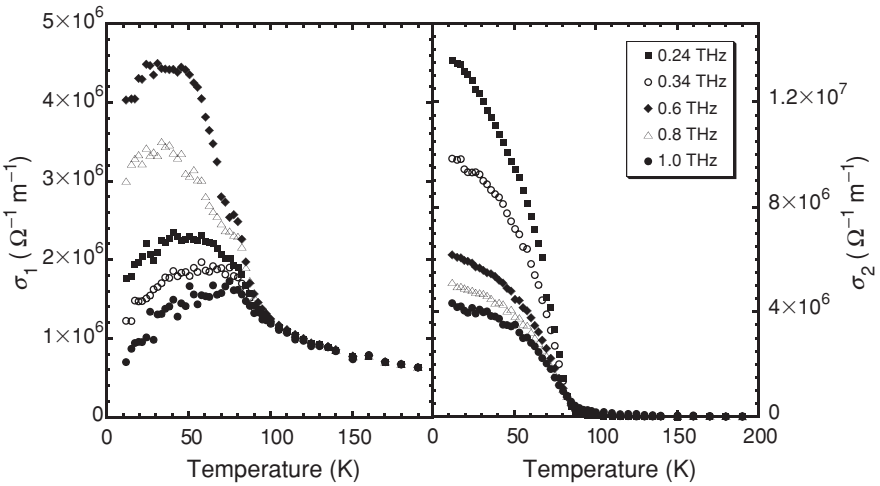

Figure 7.13. *Left panel:* σ_1 and *right panel:* σ_2 at the THz range frequencies indicated in the legend, as measured on an overdoped BSCCO thin film with $T_c = 75$ K. Here the residual conductivity is even larger than in the optimal sample, demonstrating clearly the trend that the spectral weight that remains uncondensed as $T \to 0$ is a monotonically increasing function of the hole concentration.

2. *Forcing a single component fit yields frequency dependent* ρ_n *and* τ. A useful perspective on "fitting" optical conductivity data is to recognize that the real and imaginary parts of $\sigma(\omega)$ constitute two independent observables at each frequency (although they are nonlocally related through Kramers–Kronig relations). Therefore, if the two free parameters, ρ_n and τ, are allowed to vary with ω, any $\sigma(\omega)$ can be ascribed to a single component. In a sense, this is fitting the data to an infinite number of parameters. The test, of course, is whether $\rho_n(\omega)$ and $\tau(\omega)$ turn out to be physically reasonable. When this fitting procedure is performed on the THz data, $\rho_n(\omega)$ is

found to increase by more than a factor of three from 0.8 to 0.2 THz, implying a large low-frequency renormalization of the quasiparticle mass. This seems highly unlikely in that (1) a single value of m^* is sufficient to describe $\sigma(\omega)$ in the UBC crystals and (2) ARPES yields a single value for the renormalized Fermi velocity, independent of ω and T [28].

3. *In many samples the single component description requires* $\rho_n(T)$ *to vary as* $\rho_n(0) + \alpha T$. There is no way to understand, in a mean-field picture of disorder, how $\rho_n(T)$ be singular as $T \to 0$ in the presence of a large $N(0)$.

7.3.2. Quantitative Modeling of $\sigma(\omega, T)$

Below, we describe a model for $\sigma_1(\omega, T)$ in BSCCO thin films that allows a quantitative description of the optical conductivity with a minimum of free parameters. The model posits the presence of two components of the conductivity (in addition to the condensate δ-function). The first component, which describes the entire microwave conductivity in YBCO, comes from the quasiparticles that eventually enter the condensate as $T \to 0$. The second component does not vanish in the low T limit, and indeed its spectral weight actually increases with decreasing T. Later, we will associate this component with fluctuations of the condensate phase.

To model the first component we assume the same Drude spectrum for the quasiparticle conductivity that could account for the entire $\sigma(\omega, T)$ in the case of YBCO. The spectral weight of this component is the normal fluid density that ultimately forms the condensate, which is given by $\rho_s(0) - \rho_s(T)$. We note that $\rho_n(T)$ thus defined is not a free parameter, but is determined directly from measurements of $\sigma_2(\omega, T)$. The only free parameter introduced by this component is $\tau(T)$. The measured $\sigma_1(T)$ at any one ω completely determines $\tau(T)$ and hence the predictions of the Drude model for all ω and T in the superconducting state. Figure 7.14 shows the Drude component at several frequencies, together with the data at a measurement frequency of 200 GHz. $\tau(T)$ has been determined from $\sigma_1(T)$ measured at 800 GHz, near the upper limit of the experimental range. Note that the choice of $\tau(T)$ that describes the data at 800 GHz completely fails at 200 GHz.

As a first step in modeling the additional component of the conductivity, one can compute the spectral weight left over after subtracting the Drude conductivity shown in Figure 7.14. When this subtraction is performed, it is found that the spectral weight of the remainder *increases as T is lowered*. Furthermore, the spectral weight increases in fixed proportion to the growth of the superfluid density $\rho_s(T)$. In view of the connection to the superfluid density, we refer hereafter to this contribution to $\sigma(\omega)$ as the "collective" component.

Including the collective contribution yields the following parameterization of the conductivity,

$$\sigma_1(\omega, T) = \frac{\rho_n \tau}{1 + \omega^2 \tau^2} + \frac{\kappa \rho_s / \Gamma_{cm}}{1 + \omega^2 / \Gamma_{cm}^2}. \tag{7.2}$$

In the above formula, the first term is the Drude contribution from condensing quasiparticles and the second term is another Lorentzian peak which models the collective mode. The latter introduces only two additional, T-independent parameters: κ is the fraction of $\rho_s(0)$ that remains uncondensed at $T = 0$, and Γ_{cm} is width of the uncondensed contribution.

The formulation described above provides a remarkably good description of the optical conductivity for all the samples. The comparison of the model with the measured conductivity for the optimal sample is illustrated in Figure 7.15 [20]. The collective mode parameters are $\kappa = 0.30$ and $\Gamma_{cm} = 1.5$ THz. The T-dependence of $1/\tau$ that provides the best fit to the

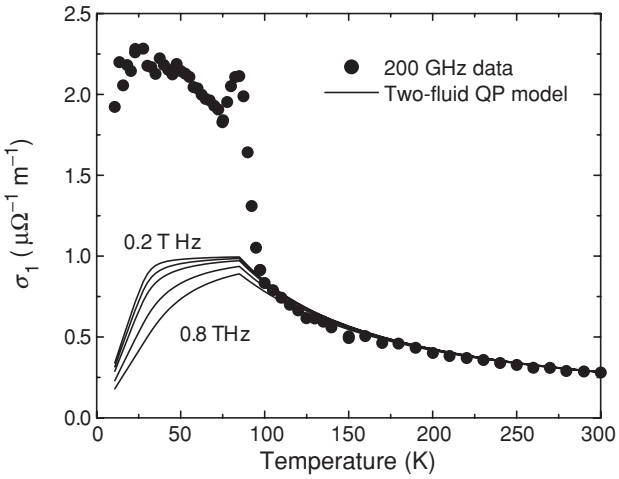

Figure 7.14. Illustration of the difficulty of modeling the measured $\sigma_1(\omega, T)$ with the Drude conductivity of thermal quasiparticles (Eq. (7.1)). *Solid lines:* Plots of Eq. (7.1) at several frequencies from 200 to 800 GHz, with $\rho_n(T)$ extracted from the measured σ_2 and $\tau(T)$ chosen to fit $\sigma_1(T)$ as measured at 800 GHz. *Solid symbols:* $\sigma_1(T)$ at 200 GHz as measured on a optimally doped BSCCO thin film.

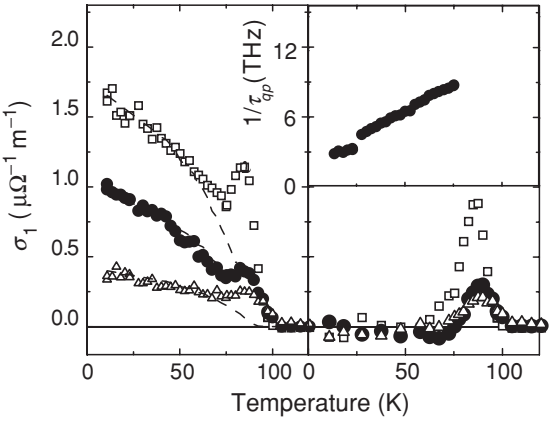

Figure 7.15. Comparison of the $2+1$ fluid model (Eq. (7.2)) with σ_1 as measured on an optimally doped BSCCO thin film. *Left panel:* Difference between the measured $\sigma_1(T)$ and quasiparticle Drude contribution (first term of Eq. (7.2)), plotted at 0.2, 0.36, and 0.64 THz as squares, circles, and triangles, respectively. The dashed lines are the collective mode conductivity (second term of Eq. (7.2)). *Lower right panel:* The difference between the measured conductivity and the best fit using Eq. (7.2) is plotted on the same scale as the left panel, and can be attributed to thermal phase fluctuations that occur in the neighborhood of T_c. *Upper right panel:* The quasiparticle scattering rate $1/\tau$, as determined from the best fit to Eq. (7.2), plotted vs. temperature with the T scale given by the panel below.

condensing quasiparticle contribution is shown in the upper right-hand panel of Figure 7.15. The left-hand panel shows the result of subtracting the quasiparticle contribution, as modeled by the first term of Eq. (7.2) from the measured conductivity. Clearly, what remains increases monotonically with decreasing T over the entire range of measurement frequency. The dashed lines indicate the values of the second term in Eq. (7.2). Finally the lower right-hand panel shows the remainder when both terms of Eq. (7.2) are subtracted from the measured

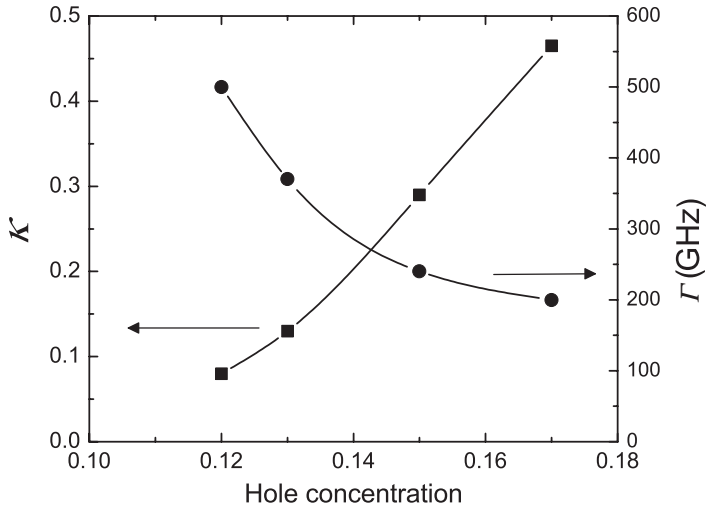

Figure 7.16. The two parameters, κ and Γ, that describe the collective mode conductivity as a function of hole concentration, δ. *Squares:* κ, the spectral weight of the collective mode expressed as a fraction of the condensate spectral weight, increases monotonically with hole concentration. *Circles:* Γ, the width of the collective mode conductivity, decreases with increasing hole concentration.

conductivity, illustrating that the model describes the data very well except for the peak near T_c that results from thermally driven superconducting fluctuations [26].

One of the main benefits of the modeling is that it facilitates comparison of the data from one sample to another. Figure 7.16 shows the variation in κ and Γ_{cm} across the measured range of hole concentration. Note that κ increases rapidly with increasing concentration, reaching almost 0.5 for the overdoped sample. The spectral weight of the collective mode contribution to σ_1 increases even more rapidly than does κ because ρ_s itself increases monotonically with x. Figure 7.17 illustrates that ρ_s increases monotonically over the measured range of hole concentration, despite the fact that T_c decreases beyond optimal doping.

7.4. Collective Mode Contribution to Optical Conductivity

7.4.1. Origin of the Collective Contribution

In Section 7.3 we showed that the optical conductivity of a set of BSCCO films could be modeled by adding to the Drude conductivity of quasiparticles a component whose spectral weight tracks $\rho_s(T)$ as T varies. The proportionality to $\rho_s(T)$ suggests a connection to current fluctuations of the condensate. However, thermal fluctuations are clearly ruled out because they decrease with decreasing T. Likewise, the quantum phase fluctuation conductivity of a spatially homogeneous superconductor, which is $\sim\sigma_Q \sim 3 \times 10^5\ \Omega^{-1}\,\mathrm{cm}^{-1}$ [29], is far too small to account for the observed conductivity.

A calculation performed by Doniach and Inui [30] suggests the conditions under which the conductivity that arises from quantum phase fluctuations can become large. The supercurrent density arising from fluctuations of the order parameter phase is given by $\vec{J}_s = \rho_s \nabla\phi$. This relationship implies that phase-fluctuation currents at wavevector q vanish in the $q \to 0$

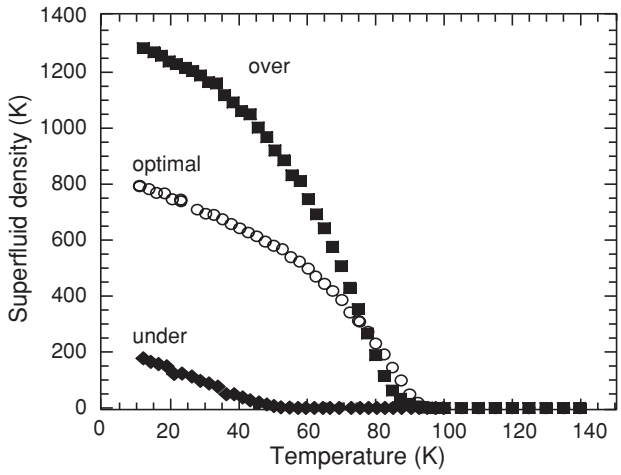

Figure 7.17. Superfluid density as a function of temperature for representative under, optimal, and overdoped BSCCO thin films. The superfluid density per Cu–O bilayer is expressed as an effective phase stiffness temperature through the relation $k_B T_\theta \equiv \hbar\omega G_2(\omega)/G_Q$, where G_2 is the imaginary part of the conductance per layer and G_Q is the conductance quantum.

limit, and therefore make no contribution to the optical conductivity. The lowest order contribution to $\sigma(\omega, q \to 0)$ arises from combined amplitude and phase fluctuations with equal but opposite wavevector, resulting in a $q = 0$ supercurrent. The fact that the current is second order in fluctuations of the order parameter leads to a small value for the conductivity. However, an implication of the Doniach and Inui calculation is that the phase fluctuation conductivity could be enhanced by quenched disorder, as static variations of the order parameter amplitude allow phase fluctuations of all wavevectors to contribute in first order to the optical conductivity.

Another argument supporting the above conclusion is the following: consider a system of clean-limit BCS superconductor islands connected by weak links with coupling J. If the islands were infinite then superfluid density would equal the entire normal state spectral weight. However, in the granular system the phase stiffness is limited by the weak links, leading to a condensate spectral weight that is only $\sim J$. In the limit that J is small, virtually the entire low-frequency spectral weight does not contribute to the superfluid density, i.e., remains uncondensed as $T \to 0$.

Barabash and Stroud [31] demonstrated that the general arguments above apply to disordered superconducting systems by considering a Josephson junction network with quenched variation δJ about the mean coupling $\bar{J}$. They showed that the global phase stiffness J is less than $\bar{J}$ (by $\langle \delta J^2 \rangle / \bar{J}$) because the phase varies more rapidly in regions where the stiffness is below the average value. The connection to optical conductivity is as follows. The spectral weight of the condensate δ-function is proportional to J, which is then less than total spectral weight of condensate current fluctuations, proportional to $\bar{J}$. Thus inhomogeneity of the superfluid density must displace spectral weight $\sim \langle \delta J^2 \rangle / \bar{J}$ from the δ-function to nonzero frequency. The fraction of spectral weight removed from the condensate (the parameter we have previously defined as κ) is therefore to be identified with $\langle \delta J^2 \rangle / \bar{J}^2$. We note that if J varies, for example with T, in such as fashion as the relative variation $\langle \sqrt{\delta J^2} \rangle / \bar{J}$ remains the same, then the fraction of the condensate weight that is displaced will also be constant.

7.4.2. Optical Conductivity in the Presence of Inhomogeneity

We have seen that, in the presence of static inhomogeneity, quantum phase fluctuations contribute substantially to the optical conductivity. To determine whether quenched inhomogeneity in ρ_s is responsible for the anomalies in $\sigma(\omega, T)$ discussed previously, we need to consider where in ω-space the spectral weight removed from the condensate will reappear. Conventional wisdom has it that, in a granular superconductor, the conductivity will appear at the natural oscillation frequency of the order parameter phase, which is the Josephson plasma frequency, ω_s. In optimal cuprates this is a very large frequency, that is $\omega_s/2\pi \sim \sqrt{\text{SWU}} \cdot 150\,\text{THz}$, whereas the anomalous dissipation is found below $\sim$1 THz. Inhomogeneity can only explain the anomalous $\sigma(\omega)$ in the cuprates if the displaced spectral weight actually appears at frequencies much smaller than ω_s.

With further reflection it is clear that the shifting of all spectral weight to ω_s is a peculiar feature of a "single-fluid" model, i.e., a superconductor with zero quasiparticle density. Consider first a disordered superconductor in which the superfluid density varies with position as $\langle\rho_s\rangle + \delta\rho_s(\vec{r})$ and $\rho_n = 0$. According to previous arguments, spectral weight $\langle\delta\rho_s^2\rangle/\langle\rho_s\rangle$ is removed from the condensate as a result of the disorder. In the neighborhood of ω_s this medium is simply a disordered conductor, and will have strong absorption bands related to the Mie absorption of small metallic particles. Therefore it is reasonable that the spectral weight removed from the condensate reappears at ω_s. Next, consider a system with the same distribution of superfluid density, but with nonzero normal fluid density distributed such that $\delta\rho_n(\vec{r}) = -\delta\rho_n(\vec{r})$. Although this system is disordered at the frequency of superconducting correlations, it is optically homogeneous near the Josephson plasma frequency (the fractional variation in optical conductivity near ω_s is $\sim 1/(\omega_p\tau)^2$). Clearly for this system the spectral weight that is shifted from the condensate cannot appear near ω_s.

The difference in the two "Gendanken samples" described above is the number of fluid components (or collective degrees of freedom). The superfluid-only sample has one collective (phase) mode which lies near the plasma frequency. On the other hand, the two-fluid medium has collective modes in which the super and normal components are either co- or counterpropagating. The counterpropagating mode will have $\nabla \cdot \vec{J} \simeq 0$ and therefore have an acoustic rather than plasmonic spectrum. We may expect that this mode will be overdamped due to the dissipation associated with the normal currents and therefore manifest as a Drude-like contribution to the optical conductivity. In Section 7.4.3. we present a model calculation [32] of the optical conductivity of a two-fluid system with quenched spatial inhomogeneity which supports the qualitative predictions discussed above.

7.4.3. Extended Two-Fluid Model

To treat the conductivity in the presence of inhomogeneity we apply the extended two-fluid phenomenology developed by Pethick and Smith [33] and Kadin and Goldman [34]. This approach successfully describes quenched inhomogeneity at the normal–superconductor interface and fluctuating inhomogeneity, as in the Carlson–Goldman oscillations [35]. In the extended two-fluid model the superfluid is accelerated by gradients of the chemical potential as well as electric fields, that is,

$$\dot{\vec{J}}_s = \rho_s(\vec{E} - \nabla[\mu_{s/e}]). \tag{7.3}$$

The chemical potential has the subscript "s" because in a superconductor μ is the energy per electron required to add a pair to the condensate. The corresponding equation for the

normal fluid current requires solving the Boltzmann equation for the quasiparticle distribution function. However, for frequencies less than $1/\tau$ the distribution function is the equilibrium distribution shifted by the "quasiparticle chemical potential" or $\mu_{\rm n}$. If the normal fluid is in local equilibrium with the condensate, $\mu_{\rm n} = \mu_{\rm s}$, which differs from "global" equilibrium where $\mu_{\rm n} = 0$. In the low-frequency regime the constitutive relation for the normal fluid has the simple form:

$$\dot{\vec{J}}_{\rm n} = \rho_{\rm n}(\vec{E} - \nabla\mu_{\rm n/e}) - \vec{J}_{\rm n}/\tau. \tag{7.4}$$

A closed system of equations requires continuity relations. The total charge of the superconductor separates naturally into a normal component, $Q_{\rm n}$, that depends on both the coherence factors and the distribution function,

$$Q_{\rm n} \equiv \sum_k q_k f_k, \tag{7.5}$$

where $q_k^2 \equiv u_k^2 - v_k^2$, and a superfluid component that depends only on coherence factors,

$$Q_{\rm s} \equiv \sum_k 2ev_k^2 = 2eN_{\rm F}\mu_{\rm s}. \tag{7.6}$$

Under conditions for which $\mu_{\rm n}$ can be defined, the normal fluid charge is given by,

$$Q_{\rm n} = 2N_{\rm F}\lambda(\mu_{\rm s} - \mu_{\rm n}), \tag{7.7}$$

where $N_{\rm F}$ is the normal state density of states at the Fermi level. The parameter λ relates the normal fluid charge to the shift of $\mu_{\rm n}$ away from local equilibrium.

In a superconducting medium the normal and superfluid charge are not separately conserved. Interconversion of normal and superconducting charge occurs through two types of processes. In the first process, $Q_{\rm n}$ changes as quasiparticles recombine or scatter. In the second, the quasiparticle charge changes even if f_k remains constant. In this process, $Q_{\rm n}$ varies because the quasiparticle excitation spectrum, and consequently the effective charge, adjusts to the local value of $\mu_{\rm s}$. Continuity equations that include both types of exchange between the two fluids are:

$$\dot{Q}_{\rm n,s} + \nabla\cdot\vec{J}_{\rm n,s} = (-,+)(\frac{Q_{\rm n}}{\tau_{\rm Q}} - \lambda\dot{Q}_{\rm s}), \tag{7.8}$$

where $\tau_{\rm Q}$ is the rate of conversion of normal charge into superfluid charge due to scattering and recombination processes. The above system of equations is closed by $\nabla\cdot\vec{E} = Q/\epsilon_0$.

To see how quenched inhomogeneity affects the optical conductivity, we consider the simplest possible model: a static one-dimensional sinusoidal variation in normal and superfluid density. We assume that the densities of the two components vary as $\rho_{\rm s,n}(x) = \langle\rho_{\rm s,n}\rangle + Re\{\rho_{{\rm s}q,{\rm n}q}{\rm e}^{{\rm i}qx}\}$, where $\langle\rho\rangle$ is the average density and ρ_q is the amplitude of the inhomogeneity at wavevector q. Because the medium is inhomogeneous, a uniform applied field generates a field at q. Solving the extended two-fluid equations to lowest order in $\rho_{{\rm n}q,{\rm s}q}$, we obtain,

$$\frac{E_q}{E_0} = -\frac{\rho_{{\rm s}q} + \rho_{{\rm n}q}F}{\omega_{\rm s}^2 - \omega^2(1-\lambda) + (\omega_{\rm n}^2 - {\rm i}\omega\lambda/\tau)F}, \tag{7.9}$$

where,

$$F \equiv \frac{\omega(\omega + {\rm i}/\tau_Q^*) - v_s^2q^2/(1-\lambda)}{(\omega+{\rm i}/\tau)(\omega+{\rm i}/\tau_Q^*) - v_{\rm n}^2q^2/\lambda}, \tag{7.10}$$

and $\omega_{\rm s,n}^2 \equiv \rho_{\rm s,n}/\epsilon_0 + v_{\rm s,n}^2q^2$, $v_{\rm s,n}^2 \equiv \rho_{\rm s,n}/2N_{\rm F}e^2$, and $\tau_{\rm Q}^* \equiv \tau_{\rm Q}(1-\lambda)$.

The uniform current density in response to these fields is given by $J_0 = \sigma_0 E_0 + \sigma_q E_{-q}$, where σ_0 is the uniform two-fluid conductivity and σ_q is the conductivity that varies with wavevector q. In the two-fluid model these are given by,

$$\sigma_{0,q} = \frac{\mathrm{i}\rho_{\mathrm{s},sq}}{\omega} + \frac{\mathrm{i}\rho_{\mathrm{n},nq}}{\omega + \mathrm{i}/\tau}. \tag{7.11}$$

The effective conductivity of the medium, $\sigma = \sigma_1 + \mathrm{i}\sigma_2$, is the ratio of the uniform current density to the uniform field, so that, $\sigma = \sigma_0 + \sigma_q E_{-q}/E_0$. The second term in this equation is the change in the optical conductivity due to inhomogeneity, or $\Delta\sigma$.

The extra term in the conductivity is particularly simple if $\rho_{\mathrm{n}} = 0$, in which case,

$$\Delta\sigma_2 = -\frac{\rho_{sq}}{\omega}\frac{\rho_{sq}}{\omega_{\mathrm{s}}^2 - \omega^2}. \tag{7.12}$$

Equation (7.12) shows that the inhomogeneity in the superfluid density indeed removes spectral weight $\rho_{sq}^2/\rho_{\mathrm{s}}$ from the condensate δ-function, in agreement with the results of [31]. In the absence of a normal fluid component the spectral weight reappears in a δ-function at the Josephson plasma frequency.

We next assume that $\rho_{\mathrm{n}} \neq 0$, and describe how this assumption affects $\Delta\sigma(\omega)$. We focus on the behavior of $\Delta\sigma$ when the normal fluid density fluctuations are either perfectly correlated or anticorrelated with those of the superfluid density. We take for two-fluid parameters values that are suggested by the terahertz and microwave experiments: $(\rho_{\mathrm{s}}/\epsilon_0)^{1/2} = 1{,}000\,\mathrm{THz}$, $(\rho_{\mathrm{n}}/\epsilon_0)^{1/2} = 800\,\mathrm{THz}$, and $\tau^{-1} = \tau_{\mathrm{Q}}^{-1} = 3\,\mathrm{THz}$. If we make the reasonable approximation of neglecting BCS coherence factors for the quasiparticle states introduced by disorder, then $\lambda = N(0)/N_{\mathrm{F}}$.

We begin with the case where the density fluctuations are perfectly anticorrelated, so that $\rho_{sq} = -\rho_{nq}$ and the total fluid density is uniform throughout the medium. Figure 7.18 shows $\Delta\sigma_1(\omega)$ with $(\rho_{sq}/\epsilon_0)^{1/2} = 100\,\mathrm{THz}$, for several values of $v_{\mathrm{s}}q\tau$. $\Delta\sigma_1(\omega)$ is positive and centered at $\omega = 0$ rather than ω_{s}. The spectra depend strongly on $v_{\mathrm{s}}q\tau$. For $v_{\mathrm{s}}q\tau \ll 1$, $\Delta\sigma_1$ has a Drude-like spectrum. As $v_{\mathrm{s}}q\tau$ increases beyond unity, the spectral weight drops and a peak near the Carlson–Goldman frequency $v_{\mathrm{s}}q$ appears in the spectrum.

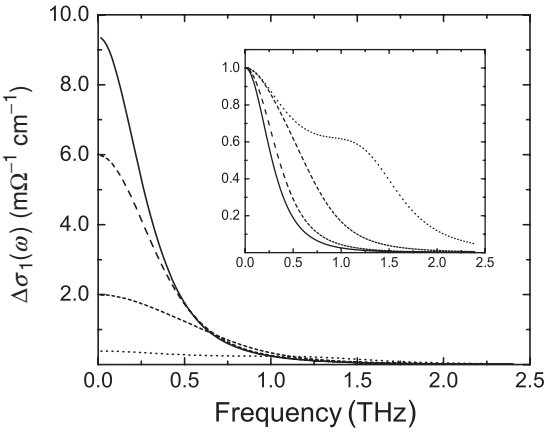

Figure 7.18. $\Delta\sigma_1$ as a function of frequency $(\omega/2\pi)$ for anticorrelated variations in ρ_{s} and ρ_{n}. Spectral weight decreases for increasing $v_{\mathrm{s}}q\tau$: 0.25, 0.5, 1.0, and 2.0. The same curves are shown in a normalized plot in the inset.

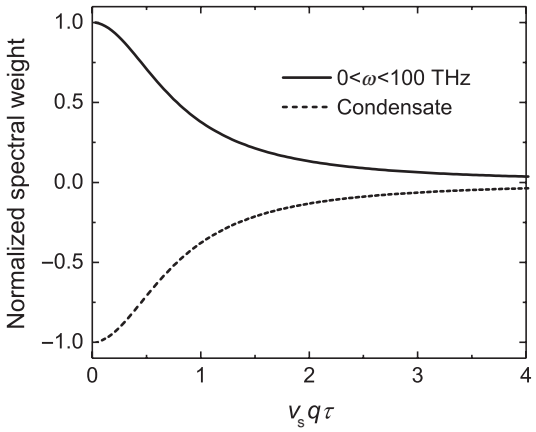

Figure 7.19. Comparison of the spectral weight displaced from the condensate by the quenched variation in ρ_s and the spectral weight that appears in $\Delta\sigma_1$ at low frequency.

The key issue is the fraction of the displaced condensate spectral weight that appears in the low-frequency peak, as opposed to frequencies near ω_s. In Figure 7.19 we compare the reduction in condensate weight with the increase in dissipation at low frequency. The change in condensate spectral weight was evaluated from the $\lim_{\omega\to 0}(\pi/2)\omega\Delta\sigma_2(\omega)$. The low-frequency spectral weight was obtained by numerically computing the integral of $\Delta\sigma_1$ with respect to ω from 0 to 100 THz. Figure 7.19 shows these two quantities, normalized to ρ_{sq}^2/ρ_s, as a function of $v_s q\tau$. They are equal in magnitude but opposite in sign, which shows that *all of the spectral weight removed from the condensate appears at low frequency and none appears at* ω_s. Moreover, the decrease of condensate spectral weight coincides exactly with the prediction of Barabash et al. [31] as $v_s q\tau \to 0$, but vanishes for $v_s q\tau \gg 1$.

The results presented above are a straightforward consequence of the anticorrelation of the density fluctuations. There is no dissipation near ω_s because the response of the medium is homogeneous at high frequencies. The anomalous dissipation appears instead at low frequency where the conductivity has strong spatial variations. σ is smaller in the regions that are superfluid poor and normal fluid rich. E will be larger in such regions, which is precisely equivalent to more rapid order parameter phase variation in regions of low stiffness. Thus the additional low-frequency dissipation arises ultimately from an amplification of E in regions with greater than average ρ_n. Finally, the dynamical inhomogeneity disappears when $q \ll (v_s\tau)^{-1}$ because the normal and superfluid response again become indistinguishable in this regime.

We are now prepared to understand the sharp difference in $\Delta\sigma$ if the super and normal fluid density waves are positively correlated. Figure 7.20 shows $\Delta\sigma_1(\omega)$ calculated with identical parameters as in Figure 7.1, except that $\rho_{sq} = \rho_{nq}$. The change in conductivity is negative, and the spectra are nearly independent of q in contrast to the strongly q dependent and positive change generated when $\rho_{sq} = -\rho_{nq}$. The reduction in conductivity is exactly as expected from the previous arguments: now regions of large E coincide with normal fluid poor regions and the dissipation is attenuated. The spectra are nearly independent of q because the dynamical inhomogeneity does not tend to zero when the normal and superfluid response become indistinguishable. The spectral weight is displaced equally from the condensate and the normal fluid, and weight $2\rho_{sq}^2/\rho_s$ shifts to very high frequency. Finally, although

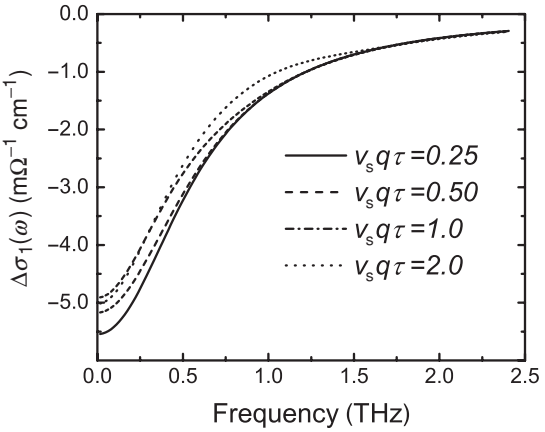

Figure 7.20. $\Delta\sigma_1$ vs. frequency for the same parameters as Figure 7.1, except variations in ρ_s and ρ_n are positively correlated.

the sensitivity of the conductivity spectrum to correlations in ρ_s and ρ_n are demonstrated for a sinusoidal distribution, the essential predictions of the above model are supported by theories that treat random spatial variations in the fluid densities [36, 37].

7.4.4. Comparison of Model and Experiment

In this section, we describe how the behavior of the optical conductivity in disordered cuprate superconductors can be readily understood in the context of the model described above. The three essential features to be explained are:

1. *Many cuprates exhibit uncondensed spectral weight at low T, suggestive of a large density of states at the chemical potential, while $\rho_s(T)$ remains linear to very low T, apparently inconsistent with large $N(0)$.*
   Point (1) is difficult to explain in a mean-field picture of a disordered d-wave superconductor because large $N(0)$ implies that as $T \to 0$ the superfluid density has the asymptotic form, $\rho_s(T) = \rho_s(0) - BT^2$. However, it *is* consistent with an inhomogeneous form of disorder in which regions of clean superconductor coexist with metallic regions that provide the large $N(0)$. Uemura has proposed superconductor/normal metal coexistence in cuprate superconductors on the basis of muon spin resonance data as well as analogies to liquid ^{3}He [38]. Such metallic regions need not have $\rho_s = 0$ as superconductivity could be induced by the proximity effect.
2. *The anomalous spectral weight appears at low frequency and, in a given sample, is proportional to $\rho_s(T)$.*
   Point (2) follows if the local values of $\rho_s(\vec{r})$ and $\rho_n(\vec{r})$ are negatively correlated, such that regions with large ρ_s have small ρ_n and vice versa.
3. *The magnitude of the low-frequency spectral weight grows monotonically as samples evolve from under to overdoped.*
   Point (3) is consistent with the picture of inhomogeneity implied by the LDOS measurements in BSCCO crystals [14, 15]. These experiments reveal a distribution of electronic properties that suggests variation in local hole concentration, x. As samples evolve from under to overdoped the mean of the distribution, $\bar{x}$, shifts toward larger values. Eventually the distribution in x should span the d-wave superconductor

(dSC)/normal metal phase boundary, with coexistence of super and normal patches an inevitable consequence. Note that the model also explains why the uncondensed spectral weight in underdoped samples appears to be small, despite the fact that the fractional variation in the local ρ_s should be just as large as in optimal or overdoped samples. In these samples the "weak links," or regions with smaller ρ_s, are not metallic. If anything their ρ_n is also smaller, so that the fluid densities are positively, rather than negatively correlated. As we saw in the previous section, in this case the order parameter phase fluctuations are not screened and the characteristic absorption appears near the plasma frequency. Indeed, this offers a possible explanation for the anomalous mid-IR absorption observed in underdoped cuprates.

7.5. Summary and Outlook

7.5.1. Summary

We have presented an overview of the microwave and millimeter wave properties of cuprate superconductors, illustrating the two types of low-frequency optical conductivity that these materials exhibit. The first type, exemplified by ultra-pure and stoichiometric YBCO single crystals, is well described by a single component originating from the Drude response of thermal quasiparticles. In other cuprate systems that have been studied $\sigma(\omega)$ has an additional component beyond the quasiparticle contribution, also centered at $\omega = 0$, with a typical width of $\sim$300 GHz. The existence of this peak has not been widely appreciated because its spectral weight lies in the gap between microwave and infrared regimes where most measurements of optical conductivity are performed. However, when microwave, terahertz, and infrared data are assembled in a composite plot, the presence of a Drude-like peak that spans these three ranges is clearly revealed. We also presented an analogous plot of the optical conductivity of ultra-pure single crystalline YBCO, in which no terahertz measurements have been performed. This composite plot reveals that the microwave conductivity does not extrapolate smoothly to the infrared conductivity, hinting at the possible presence of structure in the unmeasured region of the spectrum.

We showed that the extra component of $\sigma(\omega)$ is a collective mode that appears in the $q = 0$ response function when the order parameter amplitude, $|\Psi|$, and the density of states at the chemical potential, $N(0)$, vary with position in the medium. Such variation in microscopic parameters leads to a macroscopic description in terms of spatially varying super and normal fluid densities. A simple model of one-dimensional sinusoidal variation in ρ_s and ρ_n showed that the characteristic frequency of the collective mode depended strongly on the spatial correlation of the fluid density variations. The collective mode spectral weight appears at the low frequencies seen in experiments when the spatial variations are anticorrelated, such that the total fluid density is roughly constant in the medium. Finally, we showed that the frequency, temperature, and doping dependence of the optical conductivity in a series of BSCCO thin films could be understood to arise from the combination of a quasiparticle Drude peak and the collective mode described above.

7.5.2. Outlook and Directions of Future Research

The existence, origin, and ultimate importance of inhomogeneity are central questions facing researchers seeking to understand high-T_c superconductivity in the cuprates (see the article by Kivelson and Fradkin in this volume). The existence of strong quenched variation in

the superconducting order parameter remains an area of controversy. It has been argued that the spatial variations seen directly by STM spectroscopy are confined to the surface of the samples that have been studied [39]. Measurements of specific heat, NMR Knight shift, and fluctuations near T_c are claimed to be inconsistent with the large amplitude fluctuations seen in STM. Most relevant to optical conductivity measurements is the claim that the specific heat varies as T^2 at low temperature, with no indication of a component linear in T that could be identified with a nonzero $N(0)$ in the superconducting state. However, this conclusion is contradicted by other measurements which indicate that the linear coefficient of the specific heat, γ, does not vanish even in "high-quality" single crystalline samples [40]. Indeed the quantitative modeling of the low temperature specific heat in the cuprates is complicated, involving possible contributions from normal electrons, d-wave quasiparticles, paramagnetic centers, and phonons, all of which vanish as $T \to 0$ (see the article by Phillips in this volume). When compared to the specific heat, the optical conductivity is a much more direct probe of $N(0)$. Not only are there fewer possible contributors, but $N(0)$ appears directly as a component of the spectral weight that tends to a nonzero value as $T \to 0$.

If we interpret the combination of $\sigma(\omega)$ and STM data as solid evidence for the existence of bulk inhomogeneity in cuprate superconductors, its origin becomes the central question. This question can be framed in terms of intrinsic vs. extrinsic mechanisms, although from certain perspectives the distinction is not always clear. Extrinsic inhomogeneity is that component arising from spatial variation in the defects or chemical dopants that shift the carrier concentration away from the half-filled Mott insulating state. Intrinsic inhomogeneity occurs when CDW and/or SDW states compete with d-wave superconducting order. In the absence of disorder, intrinsic inhomogeneity is expected to vary with time, although potentially at low-frequency scales. However, the presence of chemical or structural disorder could cause quenching of low-frequency variations, generating static spatial inhomogeneity.

The crucial test for intrinsic inhomogeneity is "universality." If the spatial variations arise intrinsically from the physics of competing interactions, then they should appear in all the cuprate families of compounds. As a test for universality, measurements of low-frequency optical conductivity as a function of carrier concentration in more cuprate systems would be quite useful. Of special interest would be the $La_{2-x}Sr_xCuO_4$ system, where quenched stripe-like inhomogeneities are observed by neutron scattering [41] and large values of uncondensed spectral weight have already been reported for optimally doped samples [8].

In connection with universality, characterization of the ultra-pure and highly ordered YBCO system must been given special consideration. In mathematics, a single counter example is sufficient to disprove a conjecture. In the field of high-T_c superconductivity it is difficult to apply such rigorous logic, since experimental "truth" often changes over time. However, it seems clear that the most stringent test for intrinsic inhomogeneity would be to detect it, albeit in fluctuating form, in the cleanest of high-T_c materials. To date, interpretation of optical conductivity in the YBCO crystal system has not required invoking strong spatial inhomogeneity. The microwave conductivity is consistent with weak elastic scattering, while the infrared conductivity appears to involve Holstein-like coupling to a bosonic spectrum with energies in the 40 meV region, associated either with phonons or spin fluctuations [42]. However, the composite broadband spectra presented in Figure 7.8 show that characterization of the optical conductivity in YBCO is not complete. The missing range of the spectrum is the region above carrier scattering rates but below the gap frequency, where intrinsic fluctuations may occur. Future measurements that fill this information gap in YBCO, and extend our knowledge in other cuprate systems, will be of great value in assessing the origin and role of inhomogeneity in high-T_c superconductors.

I would like to thank Jim Eckstein and John Corson for making the study of BSCCO thin films so enjoyable, and to acknowledge valuable discussions with D.-H. Lee, J.C. Davis, S. A. Kivelson, A.J. Millis, and P.A. Lee. This work was supported by NSF-9870258 and DOE-DE-AC03-76SF00098.

Bibliography

1. P. J. Hirschfeld, W. O. Putikka, and D. J. Scalapino, Phys. Rev. Lett. **71**, 3705 (1993).
2. D. Mattis and J. Bardeen, Phys. Rev. **111**, 412 (1958).
3. A. Hosseini, R. Harris, S. Kamal, P. Dosanjh, J. Preston, R. Liang, W. N. Hardy, and D. A. Bonn, Phys. Rev. B **60**, 1349 (1999).
4. D. A. Bonn, R. Liang, T. M. Riseman, D. J. Baar, D. C. Morgan, K. Zhang, P. Dosanjh, T. L. Duty, A. MacFarlane, G. D. Morris, J. H. Brewer, et al., Phys. Rev. B **47**, 11314 (1993).
5. A. Maeda, H. Kitano, and R. Inoue, J. Phys.: Condens. Matter **17**, 143 (2005).
6. S. -F. Lee, D. C. Morgan, R. J. Ormeno, D. M. Broun, R. A. Doyle, J. R. Waldram, and K. Kadowaki, Phys. Rev. Lett. **77**, 735 (1996).
7. T. Jacobs, S. Sridhar, Q. Li, G. D. Gu, and N. Koshizuka, Phys. Rev. Lett. **75**, 4516 (1995).
8. A. V. Pronin, B. P. Gorshunov, A. A. Volkov, H. S. Somal, D. van der Marel, B. J. Feenstra, Y. Jaccard, and J. P. Locquet, JETP Lett. **68**, 6432 (1998).
9. J. Waldram, D. M. Broun, D. C. Morgan, R. Ormeno, and A. Porch, Phys. Rev. B **59**, 1528 (1999).
10. P. Hirschfeld and N. Goldenfeld, Phys. Rev. B **48**, 4219 (1993).
11. P. Lee, Phys. Rev. Lett. **71**, 1887 (1993).
12. A. Durst and P. Lee, Phys. Rev. B **62**, 1270 (2000).
13. A. Ghosal, M. Randeria, and N. Trivedi, Phys. Rev. B **65**, 014501 (2002).
14. S. H. Pan, J. P. O'Neal, R. L. Badzey, C. Chamon, H. Ding, J. R. Engelbrecht, Z. Wang, H. Eisaki, S. Uchida, A. K. Gupta, et al., Nature **413**, 282 (2001).
15. K. M. Lang, V. Madhavan, J. E. Hoffman, E. W. Hudson, H. Eisaki, S. Uchida, and J. C. Davis, Nature **415**, 412 (2002).
16. D. Bonn and W. Hardy, in *Physical Properties of High Temperature Superconductors V*, D. Ginsberg (ed.) (Singapore, World Scientific, 1996), p. 237005.
17. P. J. Turner, R. Harris, S. Kamal, M. E. Hayden, D. M. Broun, D. C. Morgan, A. Hosseini, P. Dosanjh, G. K. Mullins, J. S. Preston, et al., Phys. Rev. Lett. **90**, 237005 (2003).
18. M. C. Nuss, P. M. Mankiewich, M. L. OMalley, E. H. Westerwick, and P. B. Littlewood, Phys. Rev. Lett. **66**, 3305 (1991).
19. D. Bonn, P. Dosanjh, R. Liang, and W. N. Hardy, Phys. Rev. Lett. **68**, 2390 (1992).
20. J. Corson, J. Orenstein, S. Oh, J. O'Donnell, and J. N. Eckstein, Phys. Rev. Lett. **85**, 2569 (2000a).
21. J. Corson, J. Orenstein, J. O. S. Oh, and J. N. Eckstein, Physica B **280**, 212 (2000b).
22. J. Tu, C. Homes, G. Gu, D. Basov, S. Loureiro, R. Cava, and M. Strongin, Phys. Rev. B **66**, 144514 (2002).
23. C. C. Homes, S. V. Dordevic, D. A. Bonn, R. Liang, and W. N. Hardy, Phys. Rev. B **69**, 024514 (2004).
24. T. Shibauchi, H. Kitano, K. Uchinokura, A. Maeda, T. Kimura, and K. Kishio, Phys. Rev. Lett. **72**, 2263 (1994).
25. A. Pimenov, A. Loidl, G. Jakob, and H. Adrian, Phys. Rev. B **59**, 4390 (1999).
26. J. Corson, J. Orenstein, S. Oh, and J. Eckstein, Nature **398**, 221 (1999).
27. J. Corson, Ph.D Thesis University of California, Berkeley (2001).
28. X. J. Zhou, T. Yoshida, A. Lanzara, P. V. Bogdanov, S. A. K. K. M. Shen, W. L. Yang, F. Ronning, T. Sasagawa, T. Kakeshita, T. Noda, et al., Nature **423**, 398 (2003).
29. S. Sachdev, *Quantum Phase Transitions* (Cambridge University Press, New York, 1999).
30. S. Doniach and M. Inui, Phys. Rev. B **41**, 6668 (1990).
31. S. Barabash and D. Stroud, Phys. Rev. B **61**, 14924 (2000).
32. J. Orenstein, Physica C **67**, 144506 (2003).
33. C. Pethick and H. Smith, Ann. Phys. **119**, 133 (1979).
34. A. Kadin and A. Goldman, in *Nonequilibrium Superconductivity*, D. N. Langenberg and A. I. Larkin (ed.) (1096), p. 253.
35. R. Carlson and A. Goldman, Phys. Rev. Lett. **34**, 67 (1976).
36. J. Han, Phys. Rev. B **66**, 054517 (2002).
37. S. Barabash and D. Stroud, Phys. Rev. B **67**, 144506 (2003).

38. Y. Uemura, Solid State Commun. **126**, 23 (2003).
39. J. Loram, J. Tallon, and W. Liang, Phys. Rev. B **69**, 060502 (2004).
40. J. Emerson, D. Wright, B. Woodfield, J. Gordon, R. Fisher, and N. Phillips, Phys. Rev. Lett. **82**, 1546 (1999).
41. J. M. Tranquada, B. Sternlieb, J. Axe, Y. Nakamura, and S. Uchida, Nature **375**, 561 (1995).
42. D. Basov and T. Timusk, Rev. Mod. Phys. **48**, 4219 (2005).